HHS Public Access

Author manuscript

Neuron. Author manuscript; available in PMC 2018 July 05.

Published in final edited form as:

Neuron. 2017 July 05; 95(1): 51–62.e4. doi:10.1016/j.neuron.2017.06.002.

Selective optogenetic control of Purkinje cells in monkey cerebellum

Yasmine El-Shamayleh[1,2], **Yoshiko Kojima**[1,2], **Robijanto Soetedjo**[1,2], and **Gregory D. Horwitz**[1,2]

[1]Department of Physiology & Biophysics, University of Washington, 1959 NE Pacific St., HSB I-728, UW Mailbox 357290, Seattle, WA, 98195

[2]Washington National Primate Research Center, University of Washington, 1959 NE Pacific St., HSB I-728, UW Mailbox 357290, Seattle, WA, 98195

SUMMARY

Purkinje cells of the primate cerebellum play critical but poorly understood roles in the execution of coordinated, accurate movements. Elucidating these roles has been hampered by a lack of techniques for manipulating spiking activity in these cells selectively—a problem common to most cell types in non-transgenic animals. To overcome this obstacle, we constructed AAV vectors carrying the channelrhodopsin-2 (ChR2) gene under the control of a 1 kb L7/Pcp2 promoter. We injected these vectors into the cerebellar cortex of rhesus macaques and tested vector efficacy in three ways. Immunohistochemical analyses confirmed selective ChR2 expression in Purkinje cells. Neurophysiological recordings confirmed robust optogenetic activation. Optical stimulation of the oculomotor vermis caused saccade dysmetria. Our results demonstrate the utility of AAV–L7–ChR2 for revealing the contributions of Purkinje cells to circuit function and behavior, and they attest to the feasibility of promoter-based, targeted, genetic manipulations in primates.

eTOC

Manipulating the activity of specific neuronal types has been difficult in primates. El-Shamayleh et al. achieve selective optogenetic activation of Purkinje cells in the macaque cerebellum via AAV-mediated delivery of the ChR2 gene under control of an L7 promoter.

INTRODUCTION

The cerebellum is a phylogenetically conserved brain structure composed of distinct cell types connected by stereotyped circuitry. Purkinje cells, the sole output of the cerebellar

Corresponding author: Gregory D. Horwitz, ghorwitz@u.washington.edu.
Lead contact: Gregory D. Horwitz, ghorwitz@u.washington.edu

AUTHOR CONTRIBUTIONS

All authors contributed to study conceptualization, investigation and analysis. Y.E.S. and G.D.H. drafted the manuscript. All authors edited the manuscript.

cortex, are involved in the execution of accurate and well timed movements (Holmes, 1939; Robinson and Fuchs, 2001; Thach et al., 1992; Wolpert et al., 1998), balance and posture (Ioffe, 2013; Morton and Bastian, 2004), and learning and memory (Ito, 2002; Raymond et al., 1996). How Purkinje cells contribute to these capacities is poorly understood in large part because techniques for manipulating activity in these cells selectively are unavailable in most animal models. The inability to target these cells in non-human primates has been particularly limiting because these animals possess a combination of fine motor control, behavioral consistency, and trainability that make them particularly well suited for testing some hypotheses of Purkinje cell function.

Purkinje cell activity can be manipulated without directly affecting other cell types using optogenetics. In transgenic animals, cell type-specific targeting is relatively straightforward and requires genetic modifications early in development (for a review, see Sługocka et al., 2016). In non-transgenic animals, however, targeting is difficult. The difficulty arises from the method of gene delivery—typically viral vector injection into adult animals. These vectors carry promoter sequences that can confer a degree of cell type-specificity, but this specificity is usually modest (Kügler, 2015). Recently however, a cell type-specific promoter was used to express channelrhodopsin-2 (ChR2) selectively in dopamine neurons of rhesus macaques (Stauffer et al., 2016). Optical stimulation of these neurons produced spiking activity and caused the monkeys to make behavioral responses that they learned, over repeated trials, would trigger additional optical stimulation. The manipulation was made with a intersectional, dual-vector strategy in which one vector carried the gene for the enzyme Cre recombinase under the control of the tyrosine hydroxylase promoter (TH) and the other carried the gene for ChR2 in the FLExed (Cre-dependent) configuration (Schnütgen et al., 2003). This intersectional strategy ensured that only neurons in which the TH promoter was active produced Cre recombinase, catalyzing ChR2 expression in dopaminergic neurons selectively.

Motivated by this advance and the quest for a generalizable strategy for targeting gene delivery to specific primate neuronal types, we addressed three open questions. First, can cell type-specific promoters delivered by viral vector drive physiological levels of opsin expression directly—without a Cre-dependent strategy? A single vector approach, if sufficiently selective, would be a simpler and more efficient targeting strategy than one requiring dual transduction. Second, can cell type-specificity be achieved with a single promoter when packaged in different vector serotypes? Knowing the extent to which cell type-specificity is mediated by the promoter, as opposed to vector serotype, is critical for assessing the generalizability of this approach. Third, are cell type-specific optogenetic manipulations sufficient to affect primate behavior on single trials? Knowing the time course over which optical stimulation affects behavior constrains the hypotheses that can be tested with this technique.

To answer these questions, we expressed ChR2 in Purkinje cells of rhesus macaques using an adeno-associated viral vector (AAV) containing a 1 kb fragment of the murine L7/Pcp2 promoter (Iida et al., 2013; Oberdick et al., 1990; Tsubota et al., 2011; Yoshihara et al., 1999). We used a single vector approach that did not require Cre-dependent recombination, and we varied the vector serotype (AAV9 and AAV1). Histological analyses confirmed

Purkinje cell-specific ChR2 expression with both serotypes. Sinusoidal optical stimulation evoked vigorous, entrained spiking responses. Optical stimulation of the oculomotor vermis, triggered by saccade initiation, exerted significant and consistent effects on saccade trajectories with a latency of ~15 ms. These results demonstrate the utility of the AAV–L7–ChR2 vector for investigating the contributions of Purkinje cells to circuit function and behavior in primates, and they confirm that short promoters can mediate cell type-specific opsin expression at physiological levels in non-transgenic animals.

RESULTS

To excite Purkinje cells selectively, we engineered AAV vectors containing a 1 kb fragment of the L7/Pcp2 promoter upstream of the channelrhodopsin-2 gene (ChR2(H143R)) and injected them into the cerebellar cortex of three rhesus macaques (Figure 1). Below, we show that ChR2 expression was restricted to Purkinje cells and was sufficiently strong to mediate optically driven changes in spiking activity and saccade metrics.

Specificity of vector-mediated expression

We injected two monkeys (Monkey 1 and Monkey 2) with AAV9–L7–ChR2–mCherry. After conducting neurophysiological experiments, we processed their cerebella immunohistochemically to identify transduced cells based on mCherry expression (Figure 2A–D). Almost all mCherry-positive cells (red) were Purkinje cells as assessed by morphology, position in the Purkinje cell layer, and expression of calbindin (green), a reliable Purkinje cell marker (Fortin et al., 1998; Jande et al., 1981; Whitney et al., 2008). In contrast, few other cells were mCherry-positive (Figures S1A–B).

We quantified the selectivity and efficiency of the AAV9–L7–ChR2–mCherry vector by counting the number of mCherry-positive and calbindin-positive cells within three histological sections within the region of strongest expression (Figure 3). Selectivity, defined as the percentage of mCherry-positive cells that were also calbindin-positive, was consistently high across sections and monkeys: 91±1% for Monkey 1 and 96±2% for Monkey 2 (mean ± S.E.; Figure 3C, red). Efficiency, defined as the percentage of calbindin-positive cells over the counting region that were also mCherry-positive, was also consistently high: 72±6% for Monkey 1 and 83±3% for Monkey 2 (mean ± S.E.; Figure 3C, green). Together, these analyses show that most of the transduced cells near the injection site were Purkinje cells and that most Purkinje cells near the injection site were transduced. We inspected sixteen cells that were mCherry-positive and not calbindin-positive by confocal microscopy (63X). These cells were all located in the granule cell layer and had granule cell-like morphology (see Figure S1; images in regions corresponding to black boxes in Figure 3A–B).

We injected the second monkey (Monkey 2) with two AAV serotypes—1 and 9— containing the same L7–ChR2 construct, allowing us to compare the selectivity and efficiency of these serotypes in the same animal (Figure S2). AAV1 and AAV9 vectors had similar selectivity, both 96±2% (mean ± S.E.; Figure 3C, red), but the AAV1 vector had an efficiency of only 49±3% (mean ± S.E.; Figure 3C, green), possibly related to previous AAV1 injections made in this animal (Calcedo and Wilson, 2013; Mendoza et al., 2017, see data for Monkey F in

their Figure 6). These analyses demonstrate that Purkinje cell-specific expression of ChR2 can be achieved with either AAV1 or AAV9 vectors.

We considered the possibility that, despite their evolutionary divergence (Gao et al., 2004), AAV1 and AAV9 share a natural tropism for Purkinje cells irrespective of the promoter they carry. To control for this possibility, we injected a third monkey (Monkey 3) with AAV1–CMV–GFP, a vector driving the expression of green fluorescent protein (GFP) under control of the cytomegalovirus (CMV) promoter, which we expected to transduce cerebellar cell types less selectively (Figure 4). In this monkey, GFP expression was observed in granule cells (Figure 4A, upper white box; Figure S3A, arrows), glia (Figure 4B, lower white box; Figure S3B), and Golgi cells (Figure S3C), in addition to Purkinje cells (Figure 4B; region corresponding to middle white box in Figure 4A). Only 8% of GFP-positive cells were Purkinje cells (Figure 4C). This non-selective expression pattern shows that the Purkinje cell-specificity of the AAV1–L7–ChR2 vector was not due to the AAV1 capsid.

Optogenetic activation of Purkinje cells

We measured responses to blue (450 nm) laser light delivered via optical fiber to the cerebellar cortex. At sites where optically driven responses were evoked, we varied the frequency of optical stimulation in interleaved trials (Figure 5A). We quantified response entrainment at each frequency, fitted these data with a descriptive function and extracted two parameters: the preferred frequency and high frequency cutoff (Figure 5B). The preferred frequency of the example unit was 5 Hz (dark gray) and the high frequency cutoff was 24 Hz (light gray).

Similar results were obtained from other units. Thirty of 31 units fired more spikes during laser trials than control trials (Figure 5C). For 21 of these units, we measured the frequency dependence of optical stimulation up to 500 Hz. The average increase in spiking activity was two-fold across all laser modulation frequencies tested and was seventeen-fold at the preferred stimulation frequency (Figure 5D). Preferred stimulation frequencies ranged from 2–14 Hz (median 5 Hz), and high frequency cutoff values ranged from 3–63 Hz (median 19 Hz; Figure 5E). These data demonstrate the reliability of optogenetic activation over a broad range of stimulation frequencies.

Most units responded to light onset with a sustained increase in firing rate but did not entrain to modulations above 100 Hz. We therefore used these high frequency stimulation conditions to estimate neuronal response latencies to light steps. The latency of optogenetic activation for the example unit was 4 ms. Across the units tested (N=16), latencies ranged from 3–59 ms, with a median of 9 ms (Figure 5F). The two units with the longest latencies responded to optical stimulation with slowly ramping increases in firing rate, consistent with a polysynaptic response. These units may have been molecular layer interneurons that were disinhibited through activation of Purkinje cell axon collaterals (Witter et al., 2013).

Optogenetic control of oculomotor behavior

To probe the behavioral impact of Purkinje cell activation, we injected a fourth monkey (Monkey 4) with AAV9–L7–ChR2 in the oculomotor vermis (OMV), a midline cerebellar region identified on the basis of saccade-related bursts of neural activity (Figure S4A). The

effects of optical stimulation were assessed during visually guided saccades. On each trial, a target appeared 10° away from the fixation point along one of the cardinal directions, and on a random 50% of trials, optical stimulation was triggered by saccade initiation (Figure 6A). An example dataset from one session demonstrates the effect of stimulation on saccade trajectories (Figure 6B). Optical stimulation biased saccade endpoints to the left: rightward saccades became hypometric by 17%, and leftward saccades became hypermetric by 11%. Upward and downward saccades were also biased leftward. Additionally, downward saccades became hypermetric, an effect consistent with protraction of the deceleration phase of saccades (Figure S4B–E).

We conducted a total of 11 penetrations through the OMV and encountered light-driven responses in all of them. We conducted behavioral testing at 10 of these sites and obtained similar results each time (Figure 7A, colored lines); optical stimulation shifted saccade endpoints leftward and downward. Endpoint shifts depended on saccade direction; downward saccades were shifted primarily downward, and rightward saccades were shifted primarily leftward. All shifts were significant except for upward and downward saccades at two stimulation sites (randomization tests, $p<0.05$; see STAR Methods). The shift direction was correlated across downward, rightward, and leftward saccades (Spearman's r, $p<0.1$ for all three pairwise comparisons; e.g. downward vs. rightward). This effect was related to the position of the fiber in the OMV (Figure 7A, inset black box). At the rightmost stimulation site, saccade displacement vectors were predominantly downward. As the fiber was moved to the left, saccade displacement vectors rotated clockwise (Spearman's r between the medio-lateral position of the fiber and the angle of saccade displacement vector, $p<0.1$ for all three pairwise comparisons).

For each behavioral session, we estimated the latency of saccade deviations from velocity profiles (see STAR Methods). Latency was ~15 ms irrespective of saccade direction (Figure 7B). The latency did not depend on saccade direction or stimulation site (Kruskal-Wallis tests, $p>0.1$).

For one well-isolated OMV Purkinje cell, extracellular voltages were sampled at 50 kHz, allowing us to distinguish simple from complex spikes, the hallmark voltage waveforms of Purkinje cells (Figure S5). The rate of simple spikes increased during optical stimulation and entrained to square-wave 50 Hz laser pulses (Figure S5A; gray ticks in rasters). The rate of complex spikes, which were identified manually on the basis of waveform (see for example Figure S5B; black circles), also increased during and after optical stimulation (Figure S5A; black circles) but did not entrain to light pulses.

DISCUSSION

We constructed and vetted a viral vector (AAV–L7–ChR2) for the selective optogenetic activation of cerebellar Purkinje cells in rhesus macaques. Purkinje cell-specificity was due to the promoter (compare Figure 2, 4) not the AAV serotype (Figure 3). Optical stimulation caused spiking activity (Figure 5) and consistent changes in saccade endpoints (Figure 7). Thus, AAV–L7–ChR2 enables selective and powerful activation of Purkinje cells making it an effective tool for investigating their contributions to primate brain function and behavior.

Below, we relate our findings to previous efforts to target neuronal types in primates using cell type-specific promoters in viral vectors. We then discuss applications of this optogenetic tool for studies of cerebellar function.

Promoter-based targeting of specific cell types in primate

A key result of our study is that Purkinje cells of the monkey cerebellum can be transduced selectively by AAV vectors carrying a 1 kb L7 promoter. Such specificity is unusual for viral vector-mediated gene delivery in primates. The modest payload of viral vectors and the presumed length of cell type-specific promoters challenge the feasibility of this approach, and several attempts to achieve targeting in this way have yielded only moderate specificity (Delzor et al., 2012; Klein et al., 2016; Kügler, 2015; Nathanson et al., 2009a). However, the present study shows that some types of primate neurons can be targeted with precision using short promoters, complementing recent promising efforts described below.

Cell type-specific promoters have been used to achieve targeted transduction in non-human primates with varying degrees of success. A CaMKIIa promoter (1.3 kb) in an AAV vector was used to activate koniocellular projections from the macaque lateral geniculate nucleus to primary visual cortex, achieving a specificity of 54–88% (Klein et al., 2016). A tyrosine hydroxylase (TH) promoter (3.1 kb) in a lentiviral vector was used to target dopaminergic neurons of macaques, achieving a specificity of 96% (Lerchner et al., 2014). A shorter TH promoter (300 bp) was used in an AAV vector to drive ChR2 expression in this same neuronal type, achieving a specificity of 95% and mediating physiological and behavioral effects (Stauffer et al., 2016). A short, highly conserved gene-regulatory sequence (Dlx, 530 bp) was used to drive GFP expression in GABAergic neurons of marmosets, achieving a specificity of 93% (Dimidschstein et al., 2016). These studies, together with our current findings, provide growing support for the feasibility and promise of viral vector-mediated gene delivery to targeted neuronal classes in primate using short, cell type-specific promoters.

Our study makes three new contributions to this body of work. First, we showed for the first time that a cell type-specific promoter can drive sufficient ChR2 expression to mediate robust neuronal responses and changes in behavior. Previously, Stauffer and colleagues (2016) used a cell type-specific promoter to drive expression of Cre recombinase, which in turn, catalyzed ChR2 expression. The modularity of the Cre-dependent approach permits the use of longer promoter sequences but requires individual neurons to be transduced by two vector particles, one carrying the Cre recombinase gene and another carrying the ChR2 gene. The requirement for coincident transduction reduces efficiency compared to the single vector approach we used. Second, we showed that a cell type-specific promoter can be equally selective when packaged in different, distantly related AAV serotype capsids. Third, we showed that cell type-specific optogenetic manipulations can affect behavior on the timescale of tens of milliseconds. This result contrasts with the use of optical stimulation as a means to reinforce a learned behavior across trials (Stauffer et al., 2016). We conclude that the precise temporal control afforded by optogenetics can be exploited to manipulate the signals carried by primate Purkinje cells, a population of neurons for which spike timing is

thought to be critical for normal function (De Schutter and Steuber, 2009; Hong et al., 2016).

Potential applications of AAV–L7–ChR2

Purkinje cell spike trains have structure on multiple time scales (Bell and Grimm, 1969; De Zeeuw et al., 2008), and deciphering this temporal code will require tools that modulate Purkinje cell activity rapidly and reliably. The kinetic properties of the opsin we used, ChR2 (H134R), are ill-suited for high frequency manipulations (Tchumatchenko et al., 2013). Nevertheless, Purkinje cell responses did entrain faithfully to modulations in the 1–20 Hz range, which subsumes the frequencies produced during sinusoidal oculomotor pursuit, as well as vestibular and optokinetic stimulation protocols (Heck et al., 2013; Lisberger and Fuchs, 1978; Miles et al., 1980; Noda and Warabi, 1987; Stone and Lisberger, 1990; Suzuki and Keller, 1988). Almost all of the units we recorded followed sinusoidal optical stimulation closely; one unit had a frequency-doubled response near the preferred frequency (data not shown).

Developing optogenetic technologies that produce activity patterns that mimic natural states will facilitate interpretation of the physiological and behavioral effects that ensue. Opsins with faster kinetics will extend the range of temporal patterns that can be produced in Purkinje cells (Govorunova et al., 2017; Gunayadin et al., 2010; Klapoetke et al., 2014; Lin et al., 2009). Devices that deliver spatially patterned lights (Farah et al., 2015; Zorzos et al., 2012) will broaden the range of useful manipulations further. However, uncertainty about the spatial activity patterns that occur naturally and the convoluted structure of cerebellar cortex make this approach challenging for studying Purkinje cells.

Purkinje cells affect cerebellar output via their projections onto the deep cerebellar nuclei (DCN). However, the relationship between activity in Purkinje cells and their DCN targets is not well understood. Purkinje cells inhibit DCN neurons (Chan-Palay et al., 1982; Ito et al., 1964) but these two neuronal populations do not always modulate reciprocally (McDevitt et al., 1987), owing presumably to other inputs to the DCN (Heck et al., 2013). The temporal structure of Purkinje cell spiking is also thought to play an important role; when synchronized, Purkinje cells can increase DCN firing rates through a post-inhibitory rebound mechanism (Czubayko et al., 2001; Gauck and Jaeger, 2000; Person and Raman, 2012). Optogenetic control of Purkinje cells, with simultaneous recordings of DCN neurons, may reveal how different temporal patterns of Purkinje cell spiking modulate DCN activity. Activating Purkinje cells optogenetically during movements that modulate mossy fiber activity (Kase et al., 1980; Ohtsuka and Noda, 1992; Prsa et al., 2009; van Kan et al., 1993) may provide new insights into the interactions among pathways.

To investigate information transfer from Purkinje cells to DCN neurons directly, Purkinje cells can be optically stimulated at their axon terminals. This approach has the advantages of stimulating only the subset of Purkinje cells that innervate a region of interest in the DCN and facilitating postsynaptic response measurement. The dense axonal ChR2–mCherry expression we observed in the dentate nucleus (Figure S6), and previous successes in activating axon terminals in primates (El-Shamayleh et al., 2016; Galvan et al., 2016; Inoue et al., 2015; Klein et al., 2016), augurs well for this approach.

The DCN inhibits the inferior olive, which in turn excites Purkinje cells, creating an olivo–cerebellar loop. Signals in this circuit may account for the increase in complex spiking we observed after Purkinje cell activation (Figure S5; also see Chaumont et al., 2013; Miall et al., 1998). The long delay between optogenetic activation and increased complex spiking is consistent with the dynamics of the inhibitory synapse between the DCN and the inferior olive (Best and Regehr, 2009).

Effects of OMV Purkinje cell activation during saccades

We investigated the effect of Purkinje cell activation on saccades, a behavior that is tightly regulated by the cerebellum (Kheradmand and Zee, 2011; Robinson and Fuchs, 2001). Optical stimulation of Purkinje cells in the OMV produced robust and consistent saccade dysmetria. The robustness of this effect may be due to the fact that even modest variability in Purkinje cell firing rates can manifest in oculomotor behavior (Chaisanguanthum et al., 2014; Medina and Lisberger, 2007). The consistency of the effect suggests that optical stimulation excited populations of Purkinje cells that project to a common region of the DCN, in agreement with the coarse topography of the OMV over the region we sampled (Noda and Fujikado, 1987; Ohtsuka and Noda, 1995). Our data support the idea that Purkinje cells in the OMV contribute to saccades via the projection onto their DCN target—the caudal fastigial nucleus (cFN)—and subsequent influence on the brainstem (Kojima et al., 2014, see their Figure 8).

Optical stimulation of OMV Purkinje cells in Monkey 4 caused robust responses that waned after ~4 months of experimentation. Histological analyses revealed Purkinje cell-specific cell death in Monkey 4. This cell death is presumably due to our experimental procedures. Mechanical damage, excitotoxicity, phototoxicity, and toxicity from over-expression all may have contributed (Choi, 1987; Frigault et al., 2009; Hirase et al., 2002; Miyashita et al., 2013; Stubblefield et al., 2013; Yizhar et al., 2011), and teasing these factors apart will require experiments in which optical fiber insertion, light delivery, and opsin expression are dissociated. We note that Monkey 4 was euthanized six months after injection whereas the next-longest duration for the other monkeys was three months, consistent with the idea that cell death occurred several months after vector injection.

Optical stimulation of OMV Purkinje cells failed to evoke saccades, in contrast to electrical stimulation (Fujikado and Noda, 1987; McEligott and Keller, 1984; Noda and Fujikado, 1987; Ron and Robinson, 1973). This finding is consistent with reports of optogenetic stimulation affecting primate behavior more weakly than electrical stimulation does (Cavanaugh et al., 2012; Diester et al., 2011; Han, 2012; Han et al., 2009; Ohayon et al., 2013). Explanations for this difference include that optical stimulation activates neurons over relatively short distances (Histed et al., 2009), evokes only low frequency spiking in ChR2-positive axons (Hass and Glickfeld, 2016; Jackman et al., 2014) and does not activate afferents antidromically. Additionally, to evoke a saccade, stimulation must be strong enough to suppress omnipause neurons in the brainstem (Fuchs et al., 1985) whereas weaker stimulation is sufficient to bias saccade metrics (Keller et al., 1983; Ohtsuka and Noda, 1991).

Mid-flight optical stimulation of OMV Purkinje cells biased visually guided saccades leftwards. This result implies that stimulation was delivered to the left OMV, and is consistent with previous studies that used other techniques: electrical stimulation (Fujikado and Noda, 1987; Keller et al., 1983; McEligott and Keller, 1984; Noda and Fujikado, 1987; Ron and Robinson, 1973) and pharmacological manipulation of the OMV (Kojima et al., 2010) and the cFN (Iwamoto and Yoshida, 2002; Robinson et al., 1993; Straube et al., 2009). We found additionally that optogenetic stimulation caused downward saccades to become hypermetric. Dysmetria of upward and downward saccades has been observed in previous studies but was not emphasized perhaps due to the inconsistency of these effects (Iwamoto and Yoshida, 2002; Keller et al., 1983; Straube et al., 2009). We speculate that the consistency in the downward hypermetria we observed was due to consistency in the Purkinje cell population we stimulated optically.

Apart from being useful for oculomotor neurophysiology, Purkinje cell-specific optogenetics in primates may reveal contributions to non-motor capacities—a controversial aspect of cerebellar function (Baumann et al., 2015; Buckner, 2013; Schmahmann, 2010; Strick et al., 2009). Patients with cerebellar lesions do not exhibit gross cognitive deficits (Frank et al., 2007; Richter et al., 2005; Timmann and Daum, 2007), but convergent evidence suggests that Purkinje cell dysfunction contributes to autism spectrum disorders (Reeber et al., 2013) and schizophrenia (Andreasen and Pierson, 2008). The cerebellum has also been implicated in visual motion perception (Händel et al., 2009), interval timing (Ivry and Keele, 1989), and sequence recognition (Braitenberg et al., 1997; Molinari et al., 2008). Experiments that combine the efficacy and specificity of the AAV–L7–ChR2 vector with the sophisticated behavioral capacities of non-human primates are now poised to reveal Purkinje cell contributions to these behaviors.

STAR Methods

Contact for Reagent and Resource Sharing

Further information and requests for resources and reagents should be directed to and will be fulfilled by the Lead Contact, Gregory D. Horwitz (ghorwitz@u.washington.edu).

Experimental Model and Subject Details

Four healthy rhesus macaques (Macaca mulatta) participated in this study (two of each gender; 7–14 kg; 8–17 yrs). Monkeys were surgically implanted with a head-holding device and a recording chamber that provided access to the cerebellum. Surgical procedures, experimental protocols and animal care conformed to the NIH *Guide for the Care and Use of Laboratory Animals* and were approved by the Institutional Animal Care and Use Committee at the University of Washington.

Animal husbandry and housing were overseen by the Washington National Primate Research Center. Monkeys 1, 2 and 3 had ad-libitum access to biscuits (Fiber Plus Monkey Diet 5049, Lab Diet), and controlled daily access to fresh produce and water. Monkey 4 had ad-libitum access to water, and controlled daily access to food. When possible, animals were pair-

housed and allowed grooming contact. Cages were washed every other week, bedding was changed every day, and animals were examined by a veterinarian at least twice per year.

All four monkeys contributed to previous neurophysiological studies. Monkeys 1 and 2 contributed to studies of the primary visual cortex (Hass and Horwitz, 2013; Horwitz and Hass, 2012; Jazayeri et al., 2012; Ni et al., 2014). Monkey 3 contributed to studies of the lateral intraparietal area (Hanks et al., 2014; Kira et al., 2015). Monkey 4 contributed to studies of the superior colliculus (unpublished data). Monkey 1 had previously received injections of AAV1–hSyn–ChR2–mCherry into the primary visual cortex. Monkey 2 had previously received injections of AAV1–hSyn–oChIEF–citrine into the frontal eye fields. Monkey 4 had previously received injections of AAV1–hSyn–ChR2–mCherry into the superior colliculus. Monkey 3 was naive to AAV vectors at the time of cerebellar injections.

Method Details

Monkeys were not assigned to treatment groups by explicit randomization. No replication was performed except for the injections of AAV9–L7–ChR2–mCherry into Monkeys 1, 2, and 4. Experimenters were not blind to the vector injected.

AAV plasmid engineering and vector production—We engineered an AAV plasmid containing a promoter fragment of the Purkinje cell protein-2 (L7/Pcp2) gene (Oberdick et al., 1990; Tsubota et al., 2011; Yoshihara et al., 1999) upstream of an open reading frame consisting of Channelrhodopsin-2 (ChR2(H134R)) and mCherry coding sequences (Figure 1). A 1 kb sequence of the L7/Pcp2 promoter was amplified from a template plasmid, pBstN–L7–WGA using PCR primers: CAGGTTCCACGCGTCATGTTGGTTG (forward) and ATCGGATCCCCCTGCACGTGG (reverse). The PCR product was purified by gel electrophoresis, cut with BamH1 and Mlu1 restriction enzymes, and cloned into the pAAV–hSyn–ChR2(H134R)–mCherry plasmid using these unique restriction sites.

Recombinant AAV vectors were produced using a conventional three-plasmid transient transfection of human embryonic kidney cells (HEK 293T, female, unauthenticated) with Polyethylenimine (25 kDa, Polysciences) or calcium phosphate. Vectors were harvested and purified by ultracentrifugation through an iodixanol gradient column, exchanged into phosphate buffered saline, and titered using qPCR.

AAV vector injections—After mapping a region of the cerebellar cortex using standard extracellular recording techniques, we injected AAV vectors via a manually-advanced Hamilton syringe. Monkey 1 received 15 μl of AAV9–L7–ChR2–mCherry (1.41×10^{13}). Monkey 2 received 17 μl of AAV9–L7–ChR2–mCherry (1.41×10^{13}) and 17 μl of AAV1–L7–ChR2–mCherry. Monkey 4 received 24 μl of AAV9–L7–ChR2–mCherry (1.41×10^{13}). To provide control data, Monkey 3 received 17 μl of AAV1–CMV–GFP (6.95×10^{12}). The AAV1–CMV–GFP vector had a similar titer to the AAV1–L7–ChR2 vector to eliminate effects of discrepant titers on transduction pattern (Nathanson et al., 2009b). In Monkeys 1, 2 and 3, we injected 1 μl over 3–5 mins and waited 3–5 mins between each injection along ~10 mm tracks. In Monkey 4, four sites with strong saccade-related spiking activity were injected (~0.75 mm apart) at up to 4 depths (1.5–2 μl at each depth over the course of 1 min

with ≥ 2 mins between injections). The position and extent of transduced cerebellar regions are provided (Table 1).

Neurophysiology—Two to six weeks after injections, we searched for neuronal responses to blue light (450 nm; ~60–100 mW; sinusoidal or square-wave) delivered to the cerebellum via an optical fiber (300 μm outer diameter; Thor Labs) with a beveled tip (tapered over ~400–500 μm) that eased entry through the tentorium. A fiber and a recording electrode (Alpha Omega or FHC) were placed in a guide tube and lowered independently into the brain by microdrive. We did not vary the distance between the electrode and the optical fiber systematically but found that distances of <500 μm typically produced robust responses whereas distances of >800 μm never evoked responses. The median distance between the electrode and fiber tips was 400 μm (N=21 sites for which we had detailed positional information). Extracellular spiking activity, eye position signals (measured with scleral search coils) and other behavioral and stimulation timing events were digitized and stored for offline analysis (Plexon MAP system or Cambridge Electronics Design Power 1401 system).

Neurophysiological testing conducted in Monkeys 1 and 2 employed sinusoidally modulated optical stimulation (N=31; 11 from Monkey 1 and 20 from Monkey 2). During these sessions, animals fixated a central visual target on a computer screen in return for liquid reward. We recorded spiking activity from single units (N=12) and multiunits (N=19), obtaining qualitatively similar results regardless of isolation; we therefore pooled these data.

Behavior—Monkey 4 performed a visually guided saccade task. On each trial, the monkey fixated a 0.25° central target for 800–1000 ms, and when the target was displaced by 10° along one of the four cardinal directions, the monkey made a saccade towards the new target location. On randomly interleaved trials (50%), blue light (450 nm) was delivered to the oculomotor vermis (OMV) via optical fiber 6–9 ms after saccade initiation (when the eye velocity exceeded 15°/s) (Figure 6A). At seven of ten stimulation sites, the laser was pulsed (1.5 ms ON; 333 Hz) at 120 mW for 100 ms (i.e. 60 mW, laser power on average); at the remaining three sites, laser power was constant at 60 mW for 100 ms. Both stimulation protocols yielded qualitatively similar results, which were therefore combined.

Histology—We examined fluorescent protein expression histologically at the conclusion of neurophysiological and behavioral experiments. The number of days between vector injections and euthanasia were: 71 (Monkey 1), 85 (Monkey 2), 31 (Monkey 3) and 182 (Monkey 4). Animals were euthanized with an overdose of pentobarbital and perfused through the heart with 4% paraformaldehyde followed by a gradient of sucrose in phosphate buffer (10, 20 and 30%). The brain was extracted and cryoprotected in 30% sucrose. Sagittal sections (50 μm) were cut on a sliding microtome and mounted onto slides. Transduced cells were first localized by inspecting native fluorescence signals. Sections were then stained using primary antibodies against the reporter proteins mCherry (Clontech 632543 RRID: AB_2307319, 1:250) and GFP (Abcam 13970 RRID: AB_300798, 1:1000) and against the Purkinje cell marker calbindin (Swant CB38 RRID: AB_10000340, 1:1000), and using secondary antibodies (Invitrogen Molecular Probes): Alexa 594 (A21203 RRID: AB_141633, 1:400), Alexa 568 (A10042 RRID: AB_2534017, 1:400), Alexa 488 (A21206

RRID: AB_141708 and custom, 1:400) and the nuclear stain DAPI (Invitrogen Molecular Probes D-21490, 1:5000) for visualization by epifluorescence and confocal microscopy.

We quantified transduction selectivity and efficiency by counting mCherry-positive and calbindin-positive cells in montages imaged at 20X at the region of strongest expression in a total of eight histological sections: three from Monkey 1 and five from Monkey 2 (Figure 3 **and** Figure S2; 1031 mCherry-positive cells, 1387 calbindin-positive cells and 966 double-labeled cells). We also counted GFP-positive and calbindin-positive cells in one histological section from Monkey 3 (Figure 4; 358 GFP-positive cells, 28 calbindin-positive cells and 28 double-labeled cells). Selectivity was defined as the percentage of mCherry-positive cells that were also calbindin-positive. Efficiency was defined as the percentage of calbindin-positive cells that were also mCherry-positive. Efficiency decreases with the size of the cell counting region; we provide a single number to document the proportion of Purkinje cells that were labeled near the injection site.

We estimated the position and size of transduced regions along the anterior–posterior axis of the cerebellum by measuring the extent of fluorescent protein expression within parasagittal histological sections. We estimated the position and size of transduced regions along the medial–lateral axis, which is orthogonal to the plane of sectioning, on the basis of section morphology and the number of 50 μm sections over which fluorescence was detectable (Table 1).

Quantification and Statistical Analysis

All statistical analyses were performed in MATLAB (Mathworks, Inc.). All hypothesis testing procedures were non-parametric except for the t-tests used to determine the latency of the optical stimulation on saccade velocity (Figure 7B). A test of normality was not performed to confirm the validity of this procedure. The vectors defined by the shift in saccade endpoints due to optical stimulation had directions that were restricted to a small portion of the 0–360° range (Figure 7A), justifying use of Spearman's rank correlation coefficient to examine relationships among the following variables: saccade target location, direction of the saccade end point shift, and mediolateral position of optical fiber in craniotomy.

Neurophysiology—For each unit recorded, we analyzed rasters and peri-stimulus time histograms (PSTHs) at each laser modulation frequency (Figure 5A) to derive the summary statistics described below.

To examine the frequency dependence of optogenetic activation, we computed the response amplitude from PSTHs at each of the laser modulation frequencies tested (F1 response amplitude) and fitted these amplitudes with a log-Gaussian function (Wang and Movshon, 2016):

$$R(f)=R_0+A \bullet \exp\left[\frac{-\log\left(\frac{f}{f_p}\right)^2}{2\sigma^2}\right]$$

$R(f)$ is the response to frequency f; R_o is a vertical offset term; A is the amplitude; f_p is the preferred frequency and σ is the log-Gaussian width. From this fit, we extracted two parameters: (1) the preferred laser modulation frequency (f_p), corresponding to the maximal response amplitude and (2) the high frequency cutoff, defined as the highest frequency corresponding to half of the maximal response amplitude. We compared these parameters across the population for all units tested with the full range of frequencies, up to 500 Hz (Figure 5E; N=21). We excluded from this analysis units for which the highest frequency tested was 283 Hz (N=5 units), 129 Hz (N=2), 16 Hz (N=2), or 8 Hz (N = 1).

To evaluate the magnitude and sign of optogenetic activation, we compared the average firing rate during the first 500 ms of optical stimulation across all frequencies to the same epoch on trials without stimulation (Figure 5C). We also compared the response at the preferred stimulation frequency to the response at the same frequency on trials without stimulation (Figure 5D).

To estimate response latency to an abrupt light step, we pooled responses to 129, 222, 259, and 500 Hz stimulation conditions. We first calculated average baseline activity from the 500 ms preceding light onset and then found the first time after this interval (measured in 1 ms steps) at which average optically driven activity exceeded the average baseline activity by three standard deviations. These analyses were restricted to the subset of units that showed an increase in activity of 1.5 fold or higher at these frequencies (N=16; Figure 5E). Pooling across frequencies increased the signal-to-noise ratio of this analysis at the expense of a bias toward longer latencies; all stimuli were in sine phase and therefore reached peak intensity 1–4 ms after stimulus onset.

Behavior—To estimate the latency of optical stimulation on saccade trajectories, we identified the first time after stimulation onset that the horizontal or vertical eye velocity differed significantly between stimulation and control trials (t-tests, $p < 0.01$). The statistical significance of saccade endpoint shifts was assessed by randomization tests (10,000 resamples; Horwitz et al., 2004).

Supplementary Material

Refer to Web version on PubMed Central for supplementary material.

Acknowledgments

We thank Leah Tait and Skyler Mendoza for assistance with cloning and viral vector production, Michael Shadlen for helpful comments on the manuscript and sharing resources for viral vector production and control data collection, Christopher Fetsch and Mehdi Sanayei for help acquiring control data, Elizabeth Buffalo for generous microscope access, Rachel Wong and Anita Disney for advice on cell counting, Jing Huang for guidance in immunohistochemistry, Daniel Possin and James Kuchenbecker for guidance in histological image processing and confocal microscopy. We also thank Yoshihiro Yoshihara for the pBstN–L7–WGA plasmid and Karl Deisseroth for the pAAV–hSyn–ChR2–mCherry plasmid. This work was funded by R21EY024362 grant to G.D.H., R01EY019258 to R.S., R01EY023277 to Y. K., R01EY011378 to Michael Shadlen, NIH/ORIP grant P51OD010425 to the Washington National Primate Research Center, and NEI Center Core Grant for Vision Research P30 EY01730 to the University of Washington.

References

Andreasen NC, Pierson R. The role of the cerebellum in schizophrenia. Biol Psychiatry. 2008; 64:81–88. [PubMed: 18395701]

Baumann O, Borra RJ, Bower JM, Cullen KE, Habas C, Ivry RB, Leggio MG, Mattingley JB, Molinari M, Moulton EA, et al. Consensus paper: the role of the cerebellum in perceptual processes. Cerebellum. 2015; 14:197–220. [PubMed: 25479821]

Bell CC, Grimm RJ. Discharge properties of Purkinje cells recorded on single and double microelectrodes. J Neurophysiol. 1969; 32:1044–1055. [PubMed: 5347706]

Best AR, Regehr WG. Inhibitory regulation of electrically coupled neurons in the inferior olive is mediated by asynchronous release of GABA. Neuron. 2009; 62:555–565. [PubMed: 19477156]

Braitenberg V, Heck DH, Sultan F. The detection and generation of sequences as a key to cerebellar function: experiments and theory. Behav Brain Sci. 1997; 20:229–245. [PubMed: 10096998]

Buckner RL. The cerebellum and cognitive function: 25 years of insight from anatomy and neuroimaging. Neuron. 2013; 80:807–815. [PubMed: 24183029]

Calcedo R, Wilson JM. Humoral Immune Response to AAV. Front Immunol. 2013; 4

Cavanaugh J, Monosov IE, McAlonan K, Berman R, Smith MK, Cao V, Wang KH, Boyden ES, Wurtz RH. Optogenetic inactivation modifies monkey visuomotor behavior. Neuron. 2012; 76:901–907. [PubMed: 23217739]

Chaisanguanthum KS, Joshua M, Medina JF, Bialek W, Lisberger SG. The Neural Code for Motor Control in the Cerebellum and Oculomotor Brainstem. eNeuro. 2014; 1

Chan-Palay V, Ito M, Tongroach P, Sakurai M, Palay S. Inhibitory effects of motilin, somatostatin, [Leu]enkephalin, [Met]enkephalin, and taurine on neurons of the lateral vestibular nucleus: interactions with gamma-aminobutyric acid. Proc Natl Acad Sci U S A. 1982; 79:3355–3359. [PubMed: 6124970]

Chaumont J, Guyon N, MVA, Dugué GP, Popa D, Marcaggi P, Gautheron P, Reibel-Foisset S, Dieudonné S, Stephan A, et al. Clusters of cerebellar Purkinje cells control their afferent climbing fiber discharge. Proc Natl Acad Sci U S A. 2013; 110:16223–16228. [PubMed: 24046366]

Choi DW. Ionic dependence of glutamate neurotoxicity. J Neurosci. 1987; 7:369–379. [PubMed: 2880938]

Czubayko U, Sultan F, Thier P, Schwarz C. Two types of neurons in the rat cerebellar nuclei as distinguished by membrane potentials and intracellular fillings. J Neurophysiol. 2001; 85:2017–2029. [PubMed: 11353018]

De Schutter E, Steuber V. Patterns and pauses in Purkinje cell simple spike trains: experiments, modeling and theory. Neuroscience. 2009; 162:816–826. [PubMed: 19249335]

De Zeeuw CI, Hoebeek FE, Schonewille M. Causes and consequences of oscillations in the cerebellar cortex. Neuron. 2008; 58:655–658. [PubMed: 18549777]

Delzor A, Dufour N, Petit F, Guillermier M, Houitte D, Auregan G, Brouillet E, Hantraye P, Délgon N. Restricted transgene expression in the brain with cell-type specific neuronal promoters. Hum Gene Ther Methods. 2012; 23:242–254. [PubMed: 22934828]

Diester I, Kaufman MT, Mogri M, Pashaie R, Goo W, Yizhar O, Ramakrishnan C, Deisseroth K, Shenoy KV. An optogenetic toolbox designed for primates. Nat Neurosci. 2011; 14:387–397. [PubMed: 21278729]

Dimidschstein J, Chen Q, Tremblay R, Rogers SL, Saldi GA, Guo L, Xu Q, Liu R, Lu C, Chu J, et al. A viral strategy for targeting and manipulating interneurons across vertebrate species. Nat Neurosci. 2016; 19:1743–1749. [PubMed: 27798629]

El-Shamayleh Y, Ni AM, Horwitz GD. Genetic strategies for targeting primate neural circuits. J Neurophysiol. 2016; 116:122–134. [PubMed: 27052579]

Farah N, Levinsky A, Brosh I, Kahn I, Shoham S. Holographic fiber bundle system for patterned optogenetic activation of large-scale neuronal networks. Neurophotonics. 2015; 2:045002. [PubMed: 26793741]

Fortin M, Marchand R, Parent A. Calcium-binding proteins in primate cerebellum. Neuroscie Res. 1998; 30:155–168.

Frank B, Schoch B, Richter S, Frings M, Karnath HO, Timmann D. Cerebellar lesion studies of cognitive function in children and adolescents - limitations and negative findings. Cerebellum. 2007; 6:242–253. [PubMed: 17786821]

Frigault MM, Lacoste J, Swift JL, Brown CM. Live-cell microscopy - tips and tools. J Cell Sci. 2009; 122:753–767. [PubMed: 19261845]

Fuchs AF, Kaneko CR, Scudder CA. Brainstem control of saccadic eye movements. Annu Rev Neurosci. 1985; 8:307–337. [PubMed: 3920944]

Fujikado T, Noda H. Saccadic eye movements evoked by microstimulation of lobule VII of the cerebellar vermis of macaque monkeys. J Physiol. 1987; 394:573–594. [PubMed: 3443975]

Galvan A, Hu X, Smith Y, Wichmann T. Effects of Optogenetic Activation of Corticothalamic Terminals in the Motor Thalamus of Awake Monkeys. J Neurosci. 2016; 36:3519–3530. [PubMed: 27013680]

Gao G, Vandenberghe LH, Alvira MR, Lu Y, Calcedo R, Zhou X, Wilson JM. Clades of Adeno-associated viruses are widely disseminated in human tissues. J Virol. 2004; 78:6381–6388. [PubMed: 15163731]

Gauck V, Jaeger D. The control of rate and timing of spikes in the deep cerebellar nuclei by inhibition. J Neurosci. 2000; 20:3006–3016. [PubMed: 10751453]

Govorunova EG, Sineshchekov OA, Rodarte EM, Janz R, Morelle O, Melkonian M, Wong GK, Spudich JL. The Expanding Family of Natural Anion Channelrhodopsins Reveals Large Variations in Kinetics, Conductance, and Spectral Sensitivity. Sci Rep. 2017; 7

Gunayadin LA, Yizhar O, Berndt A, Sohal VS, Deisseroth K, Hegemann P. Ultrafast optogenetic control. Nat Neurosci. 2010; 13:387–392. [PubMed: 20081849]

Han X. Optogenetics in the nonhuman primate. Prog Brain Res. 2012; 196:215–233. [PubMed: 22341328]

Han X, Qian X, Zhou HH, Franzesi GT, Stern P, Bronson RT, Graybiel AM, Desimone R, Boyden ES. Millisecond-timescale optical control of neural dynamics in the nonhuman primate brain. Neuron. 2009; 62:191–198. [PubMed: 19409264]

Händel B, Thier P, Haarmeier T. Visual motion perception deficits due to cerebellar lesions are paralleled by specific changes in cerebro-cortical activity. J Neurosci. 2009; 29:15126–15133. [PubMed: 19955364]

Hanks T, Kiani R, Shadlen MN. A neural mechanism of speed-accuracy tradeoff in macaque area LIP. Elife. 2014; 27

Hass CA, Glickfeld LL. High-fidelity optical excitation of cortico-cortical projections at physiological frequencies. J Neurophysiol. 2016; 116:2056–2066. [PubMed: 27489370]

Hass CA, Horwitz GD. V1 mechanisms underlying chromatic contrast detection. J Neurophysiol. 2013; 109:2483–2494. [PubMed: 23446689]

Heck DH, De Zeeuw CI, Jaeger D, Khodakhah K, Person AL. The neuronal code(s) of the cerebellum. J Neurosci. 2013; 33:17603–17609. [PubMed: 24198351]

Hirase H, Nikolenko V, Goldberg JH, Yuste R. Multiphoton stimulation of neurons. J Neurobiol. 2002; 51:237–247. [PubMed: 11984845]

Histed MH, Bonin V, Reid RC. Direct activation of sparse, distributed populations of cortical neurons by electrical microstimulation. Neuron. 2009; 63:508–522. [PubMed: 19709632]

Holmes G. The cerebellum of man. Brain Res. 1939; 62:1–30.

Hong S, Negrello M, Junker M, Smilgin A, Thier P, De Schutter E. Multiplexed coding by cerebellar Purkinje neurons. Elife. 2016; 5

Horwitz GD, Batista AP, Newsome WT. Representation of an abstract perceptual decision in macaque superior colliculus. J Neurophysiol. 2004; 91:2281–2296. [PubMed: 14711971]

Horwitz GD, Hass CA. Nonlinear analysis of macaque V1 color tuning reveals cardinal directions for cortical color processing. Nat Neurosci. 2012; 15:913–919. [PubMed: 22581184]

Iida A, Takino N, Miyauchi H, Shimazaki K, Muramatsu S. Systemic delivery of tyrosine-mutant AAV vectors results in robust transduction of neurons in adult mice. Biomed Res Int. 2013; 2013

Inoue K, Takada M, Matsumoto M. Neuronal and behavioural modulations by pathway-selective optogenetic stimulation of the primate oculomotor system. Nat Commun. 2015; 6

Ioffe, ME. Springer. Handbook of the cerebellum and cerebellar disorders. New York: 2013. Cerebellar control of posture; p. 1221-1240.

Ito M. Historical review of the significance of the cerebellum and the role of Purkinje cells in motor learning. Ann N Y Acad Sci. 2002; 978:273–288. [PubMed: 12582060]

Ito M, Yoshida M, Obata K. Monosynaptic inhibition of the intracerebellar nuclei induced from the cerebellar cortex. Experientia. 1964; 20:575–576. [PubMed: 5859224]

Ivry RB, Keele SW. Timing functions of the cerebellum. J Cogn Neurosci. 1989; 1:136–152. [PubMed: 23968462]

Iwamoto Y, Yoshida K. Saccadic dysmetria following inactivation of the primate fastigial oculomotor region. Neurosci Lett. 2002; 325:211–215. [PubMed: 12044658]

Jackman SL, Beneduce BM, Drew IR, Regehr WG. Achieving high-frequency optical control of synaptic transmission. J Neurosci. 2014; 34:7704–7714. [PubMed: 24872574]

Jande SS, Maler L, Lawson DE. Immunohistochemical mapping of vitamin D-dependent calcium-binding protein in brain. Nature. 1981; 294

Jazayeri M, Lindbloom-Brown Z, Horwitz GD. Saccadic eye movements evoked by optogenetic activation of primate V1. Nat Neurosci. 2012; 15:1368–1370. [PubMed: 22941109]

Kase M, Miller DC, Noda H. Discharges of Purkinje cells and mossy fibres in the cerebellar vermis of the monkey during saccadic eye movements and fixation. J Physiol. 1980; 300:539–555. [PubMed: 6770085]

Keller EL, Slakey DP, Crandall WF. Microstimulation of the primate cerebellar vermis during saccadic eye movements. Brain Res. 1983; 288:131–143. [PubMed: 6661614]

Kheradmand A, Zee DS. Cerebellum and ocular motor control. Front Neurol. 2011; 2

Kira S, Yang T, Shadlen MN. A neural implementation of Wald's sequential probability ratio test. Neuron. 2015; 85:861–873. [PubMed: 25661183]

Klapoetke NC, Murata Y, Kim SS, Pulver SR, Birdsey-Benson A, Cho YK, Morimoto TK, Chuong AS, Carpenter EJ, Tian Z, et al. Independent optical excitation of distinct neural populations. Nat Methods. 2014; 11:338–346. [PubMed: 24509633]

Klein C, Evrard HC, Shapcott KA, Haverkamp S, Logothetis NK, Schmid MC. Cell-Targeted Optogenetics and Electrical Microstimulation Reveal the Primate Koniocellular Projection to Supra-granular Visual Cortex. Neuron. 2016; 90:143–151. [PubMed: 27021172]

Kojima Y, Robinson FR, Soetedjo R. Cerebellar fastigial nucleus influence on ipsilateral abducens activity during saccades. J Neurophysiol. 2014; 111:1553–1563. [PubMed: 24478158]

Kojima Y, Soetedjo R, Fuchs AF. Effects of GABA agonist and antagonist injections into the oculomotor vermis on horizontal saccades. Brain Res. 2010; 1366:93–100. [PubMed: 20951682]

Kügler, S. Gene Therapy for Neurological Disorders: Methods and Protocols. New York: Springer; 2015. Tissue-specific promoters in the CNS; p. 81-91.

Lerchner W, Corigat B, Der Minassian V, Saunders RC, Richmond BJ. Injection parameters and virus dependent choice of promoters to improve neuron targeting in the nonhuman primate brain. Gene Ther. 2014; 21:233–241. [PubMed: 24401836]

Lin JY, Lin MZ, Steinbach P, Tsien RY. Characterization of engineered channelrhodopsin variants with improved properties and kinetics. Biophys J. 2009; 96:1803–1814. [PubMed: 19254539]

Lisberger SG, Fuchs AF. Role of primate flocculus during rapid behavioral modification of vestibuloocular reflex. I. Purkinje cell activity during visually guided horizontal smooth-pursuit eye movements and passive head rotation. J Neurophysiol. 1978; 41:733–763. [PubMed: 96225]

Madigan, JC., Carpenter, MB. Cerebellum of the rhesus monkey; atlas of lobules, laminae, and folia, in sections. Baltimore: University Park Press; 1971.

McDevitt CJ, Ebner TJ, Bloedel JR. Relationships between simultaneously recorded Purkinje cells and nuclear neurons. Brain Res. 1987; 425:1–13. [PubMed: 3427412]

McEligott JG, Keller EL. Cerebellar vermis involvement in monkey saccadic eye movements: microstimulation. Exp Neurol. 1984; 86:543–558. [PubMed: 6499993]

Medina JF, Lisberger SG. Variation, signal, and noise in cerebellar sensory-motor processing for smooth-pursuit eye movements. J Neurosci. 2007; 27:6832–6842. [PubMed: 17581971]

Mendoza SM, El-Shamayleh Y, Horwitz GD. AAV-mediated delivery of optogenetic constructs to the macaque brain triggers humoral immune responses. J Neurophysiol. 2017; 117:2004–2013. [PubMed: 28202570]

Miall RC, Keating JG, Malkmus M, Thach WT. Simple spike activity predicts occurrence of complex spikes in cerebellar Purkinje cells. Nat Neurosci. 1998; 1:13–15. [PubMed: 10195101]

Miles FA, Braitman DJ, Dow BM. Long-term adaptive changes in primate vestibuloocular reflex. IV. Electrophysiological observations in flocculus of adapted monkeys. J Neurophysiol. 1980; 43:1477–1493. [PubMed: 6768854]

Miyashita T, Shao YR, Chung J, Pourzia O, Feldman DE. Long-term channelrhodopsin-2 (ChR2) expression can induce abnormal axonal morphology and targeting in cerebral cortex. Front Neural Circuits. 2013; 7

Molinari M, Chiricozzi FR, Clausi S, Tedesco AM, De Lisa M, Leggio MG. Cerebellum and detection of sequences, from perception to cognition. Cerebellum. 2008; 7:611–615. [PubMed: 18941861]

Morton SM, Bastian AJ. Cerebellar control of balance and locomotion. Neuroscientist. 2004; 10:247–259. [PubMed: 15155063]

Nathanson JL, Jappelli R, Scheef ED, Manning G, Obata K, Brenner S, Callaway EM. Short Promoters in Viral Vectors Drive Selective Expression in Mammalian Inhibitory Neurons, but do not Restrict Activity to Specific Inhibitory Cell-Types. Front Neural Circuits. 2009a; 3

Nathanson JL, Yanagawa Y, Obata K, Callaway EM. Preferential labeling of inhibitory and excitatory cortical neurons by endogenous tropism of adeno-associated virus and lentivirus vectors. Neuroscience. 2009b; 161:441–450. [PubMed: 19318117]

Ni AM, Murray SO, Horwitz GD. Object-centered shifts of receptive field positions in monkey primary visual cortex. Curr Biol. 2014; 24:1653–1658. [PubMed: 25017208]

Noda H, Fujikado T. Involvement of Purkinje cells in evoking saccadic eye movements by microstimulation of the posterior cerebellar vermis of monkeys. J Neurophysiol. 1987; 57:1247–1261. [PubMed: 3585467]

Noda H, Warabi T. Responses of Purkinje cells and mossy fibres in the flocculus of the monkey during sinusoidal movements of a visual pattern. J Physiol. 1987; 387:611–628. [PubMed: 3656184]

Oberdick J, Smeyne RJ, Mann JR, Zackson S, Morgan JI. A promoter that drives transgene expression in cerebellar Purkinje and retinal bipolar neurons. Science. 1990; 248:223–226. [PubMed: 2109351]

Ohayon S, Grimaldi P, Schweers N, Tsao DY. Saccade modulation by optical and electrical stimulation in the macaque frontal eye field. J Neurosci. 2013; 33:16684–16697. [PubMed: 24133271]

Ohtsuka K, Noda H. The effect of microstimulation of the oculomotor vermis on discharges of fastigial neurons and visually-directed saccades in macaques. Neurosci Res. 1991; 10:290–295. [PubMed: 1652724]

Ohtsuka K, Noda H. Burst discharges of mossy fibers in the oculomotor vermis of macaque monkeys during saccadic eye movements. Neurosci Res. 1992; 15:102–114. [PubMed: 1336577]

Ohtsuka K, Noda H. Discharge properties of Purkinje cells in the oculomotor vermis during visually guided saccades in the macaque monkey. J Neurophysiol. 1995; 74:1828–1840. [PubMed: 8592177]

Person AL, Raman IM. Synchrony and neural coding in cerebellar circuits. Front Neural Circuits. 2012; 6

Prsa M, Dash S, Catz N, Dicke PW, Thier P. Characteristics of responses of Golgi cells and mossy fibers to eye saccades and saccadic adaptation recorded from the posterior vermis of the cerebellum. J Neurosci. 2009; 29:250–262. [PubMed: 19129401]

Raymond JL, Lisberger SG, Mauk MD. The cerebellum: a neuronal learning machine? Science. 1996; 272:1126–1131. [PubMed: 8638157]

Reeber SL, Otis TS, Sillitoe RV. New roles for the cerebellum in health and disease. Front Syst Neurosci. 2013; 7

Richter S, Schoch B, Kaiser O, Groetschel H, Hein-Kropp C, Maschke M, Dimitrova A, Gizewski E, Ziegler W, Karnath HO, et al. Children and adolescents with chronic cerebellar lesions show no clinically relevant signs of aphasia or neglect. J Neurophysiol. 2005; 94:4180–4120.

Robinson FR, Fuchs AF. The role of the cerebellum in voluntary eye movements. Annu Rev Neurosci. 2001; 24:981–1004. [PubMed: 11520925]

Robinson FR, Straube A, Fuchs AF. Role of the caudal fastigial nucleus in saccade generation. II. Effects of muscimol inactivation. J Neurophysiol. 1993; 70:1741–1758. [PubMed: 8294950]

Ron S, Robinson DA. Eye movements evoked by cerebellar stimulation in the alert monkey. J Neurophysiol. 1973; 36:1004–1022. [PubMed: 4202613]

Schmahmann JD. The role of the cerebellum in cognition and emotion: personal reflections since 1982 on the dysmetria of thought hypothesis, and its historical evolution from theory to therapy. Neuropsychol Rev. 2010; 20:236–260. [PubMed: 20821056]

Schnütgen F, Doerflinger N, Calléja C, Wendling O, Chambon P, Ghyselinck NB. A directional strategy for monitoring Cre-mediated recombination at the cellular level in the mouse. Nat Biotechnol. 2003; 21:562–565. [PubMed: 12665802]

Sługocka A, Wiaderkiewicz J, Barski JJ. Genetic Targeting in Cerebellar Purkinje Cells: an Update. Cerebellum. 2016:1–12. [PubMed: 26744149]

Stauffer WR, Lak A, Yang A, Borel M, Paulsen O, Boyden ES, Schultz W. Dopamine Neuron-Specific Optogenetic Stimulation in Rhesus Macaques. Cell. 2016; 166:1564–1571. [PubMed: 27610576]

Stone LS, Lisberger SG. Visual responses of Purkinje cells in the cerebellar flocculus during smooth-pursuit eye movements in monkeys. I. Simple spikes. J Neurophysiol. 1990; 63:1241–1261. [PubMed: 2358872]

Straube A, Scheuerer W, Robinson FR, Eggert T. Temporary lesions of the caudal deep cerebellar nucleus in nonhuman primates. Gain, offset, and ocular alignment. Ann N Y Acad Sci. 2009; 1164:119–126. [PubMed: 19645889]

Strick PL, Dum RP, Fiez JA. Cerebellum and nonmotor function. Annu Rev Neurosci. 2009; 32:413–434. [PubMed: 19555291]

Stubblefield EA, Costabile JD, Felsen G. Optogenetic investigation of the role of the superior colliculus in orienting movements. Behav Brain Res. 2013; 255:55–63. [PubMed: 23643689]

Suzuki DA, Keller EL. The role of the posterior vermis of monkey cerebellum in smooth-pursuit eye movement control. II. Target velocity-related Purkinje cell activity. J Neurophysiol. 1988; 59:19–40. [PubMed: 3343601]

Tchumatchenko T, Newman JP, Fong MF, Potter SM. Delivery of continuously-varying stimuli using channelrhodopsin-2. Front Neural Circuits. 2013; 7

Thach WT, Goodkin HP, Keating JG. The cerebellum and the adaptive coordination of movement. Annu Rev Neurosci. 1992; 15:403–442. [PubMed: 1575449]

Timmann D, Daum I. Cerebellar contributions to cognitive functions: a progress report after two decades of research. Cerebellum. 2007; 6:159–162. [PubMed: 17786810]

Tsubota T, Ohashi Y, Tamura K, Sato A, Miyashita Y. Optogenetic manipulation of cerebellar Purkinje cell activity in vivo. PLoS One. 2011; 6

van Kan PL, Gibson AR, Houk JC. Movement-related inputs to intermediate cerebellum of the monkey. J Neurophysiol. 1993; 69:74–94. [PubMed: 8433135]

Wang HX, Movshon JA. Properties of pattern and component direction-selective cells in area MT of the macaque. J Neurophysiol. 2016; 115:2705–2720. [PubMed: 26561603]

Whitney ER, Kemper TL, Rosene DL, Bauman ML, Blatt GJ. Calbindin-D28k is a more reliable marker of human Purkinje cells than standard Nissl stains: a stereological experiment. J Neurosci Methods. 2008; 168:42–47. [PubMed: 17961663]

Witter L, Canto CB, Hoogland TM, de Gruijl JR, De Zeeuw CI. Strength and timing of motor responses mediated by rebound firing in the cerebellar nuclei after Purkinje cell activation. Front Neural Circuits. 2013; 7

Wolpert DM, Miall RC, Kawato M. Internal models in the cerebellum. Trends Cogn Sci. 1998; 2:338–347. [PubMed: 21227230]

Yizhar O, Fenno LE, Davidson TJ, Mogri M, Deisseroth K. Optogenetics in neural systems. Neuron. 2011; 71:9–34. [PubMed: 21745635]

Yoshihara Y, Mizuno T, Nakahira M, Kawasaki M, Watanabe Y, Kagamiyama H, Jishage K, Ueda O, Suzuki H, Tabuchi K, et al. A genetic approach to visualization of multisynaptic neural pathways using plant lectin transgene. Neuron. 1999; 22:33–41. [PubMed: 10027287]

Zorzos AN, Scholvin J, Boyden ES, Fonstad CG. Three-dimensional multiwaveguide probe array for light delivery to distributed brain circuits. Opt Lett. 2012; 37:4841–4843. [PubMed: 23202064]

Highlights

- An L7 promoter in AAV vectors directed ChR2 expression to macaque Purkinje cells.
- Sinusoidal illumination of ChR2+ cells drove vigorous, entrained spiking responses.
- Activation of Purkinje cells in the oculomotor vermis biased saccade trajectories.

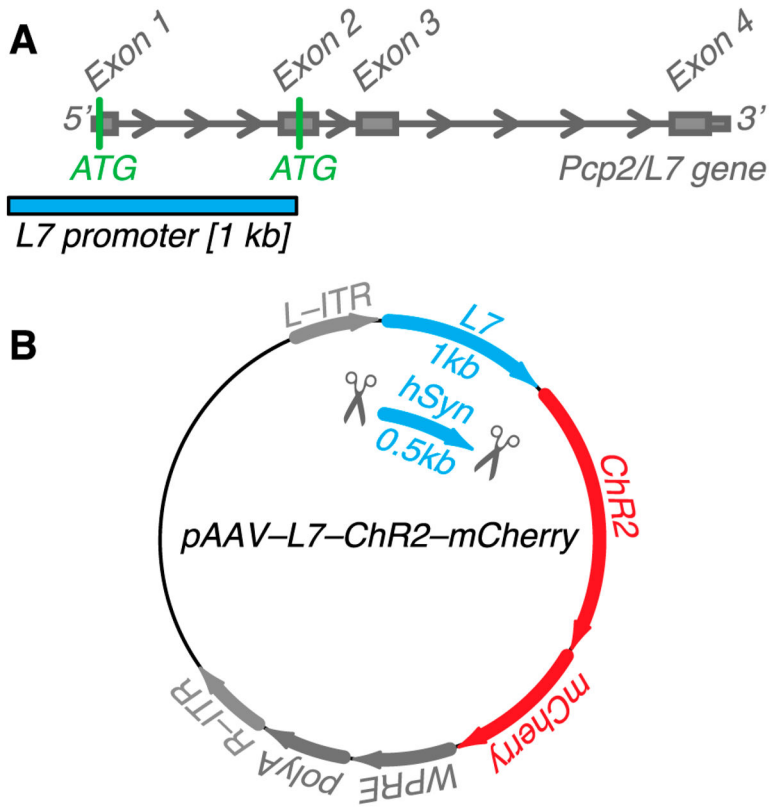

Figure 1.

AAV plasmid cloning. **(A)** The L7/Pcp2 promoter fragment is shown in relationship to the L7/Pcp2 gene model; this fragment corresponds to the 1 kb sequence upstream of the ATG in Exon 2. **(B)** The promoter fragment was cloned upstream of an open reading frame consisting of Channelrhodopsin-2 (ChR2(H134R)) and mCherry coding sequences, replacing the human synapsin promoter (hSyn, 0.5 kb).

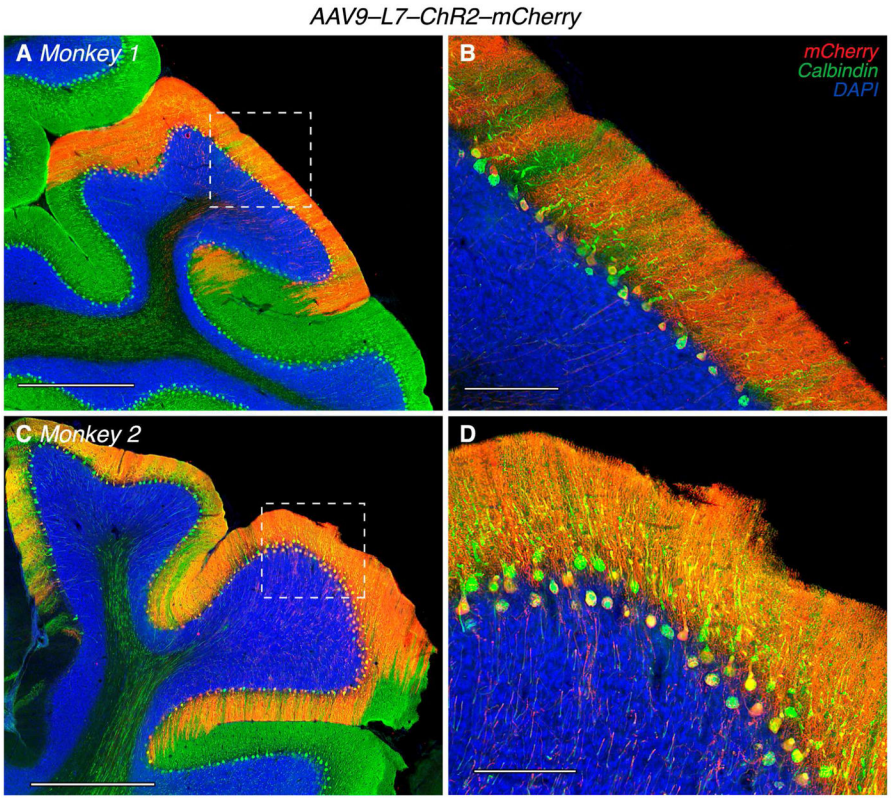

Figure 2.

Transduction pattern of AAV9–L7–ChR2–mCherry. **(A,C)** 10X montages of two histological sections from Monkey 1 and Monkey 2. Scale bars are 1000 μm. **(B,D)** 20X montages of the same sections as **A,C,** corresponding to regions outlined by the dashed white boxes. Scale bars are 200 μm. Most of the modest mCherry labeling in the granule cell layer is due to Purkinje cell axons.

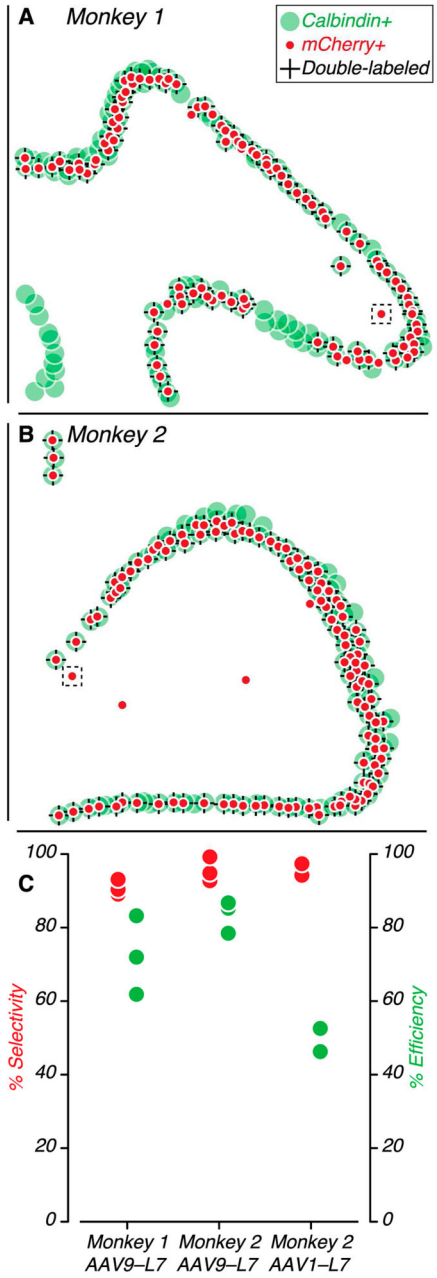

Figure 3.

Selectivity and efficiency of transduction. **(A–B)** Schematic of cell counts for two histological sections (same as in Figure 2). Calbindin-positive cells are green, mCherry-positive cells are red, and double-labelled cells are denoted by "+"s. Regions outlined by the dashed black boxes are shown in Figure S1. **(C)** Selectivity (left ordinate, red) and efficiency (right ordinate, green) values for each histological section examined.

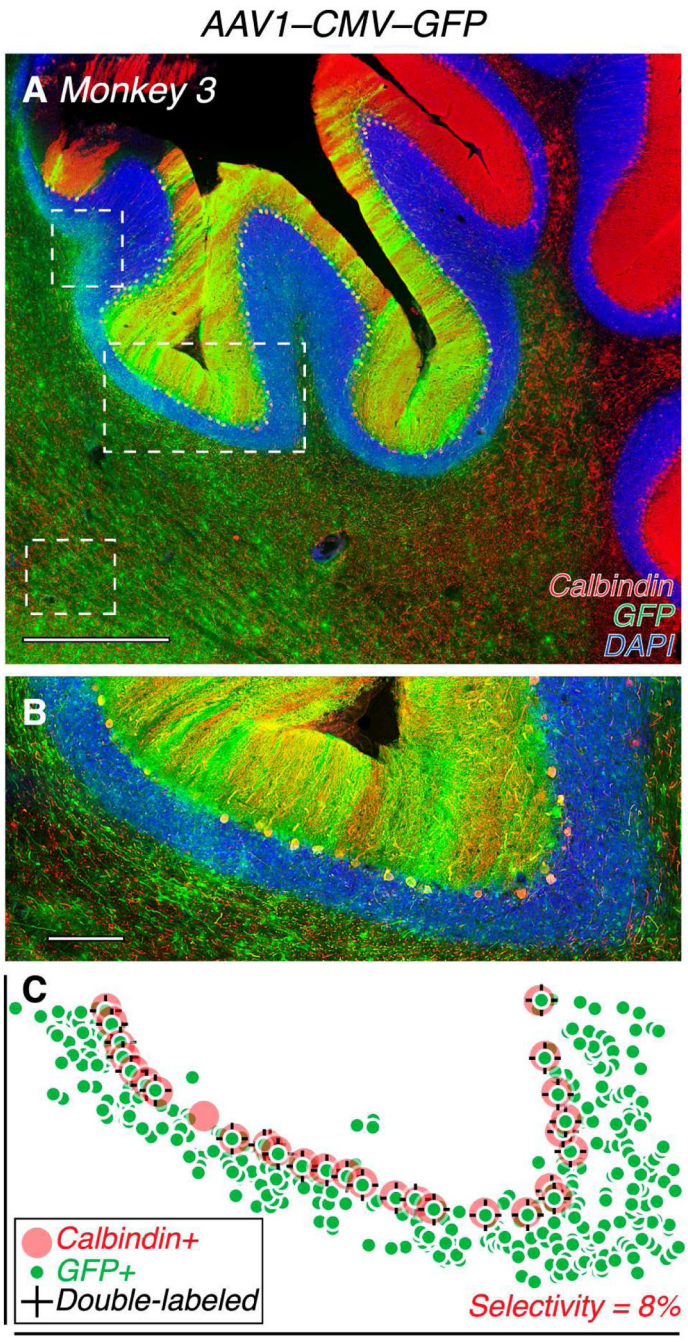

Figure 4.

Transduction pattern of AAV1–CMV–GFP. **(A)** 10X montages of one histological section from Monkey 3. Scale bar is 1000 μm. **(B)** 20X montages of the same sections as **A**, corresponding to the region outlined by the largest dashed white box. Scale bar is 200 μm. Regions outlined by the smaller dashed white boxes are shown in Figure S3.

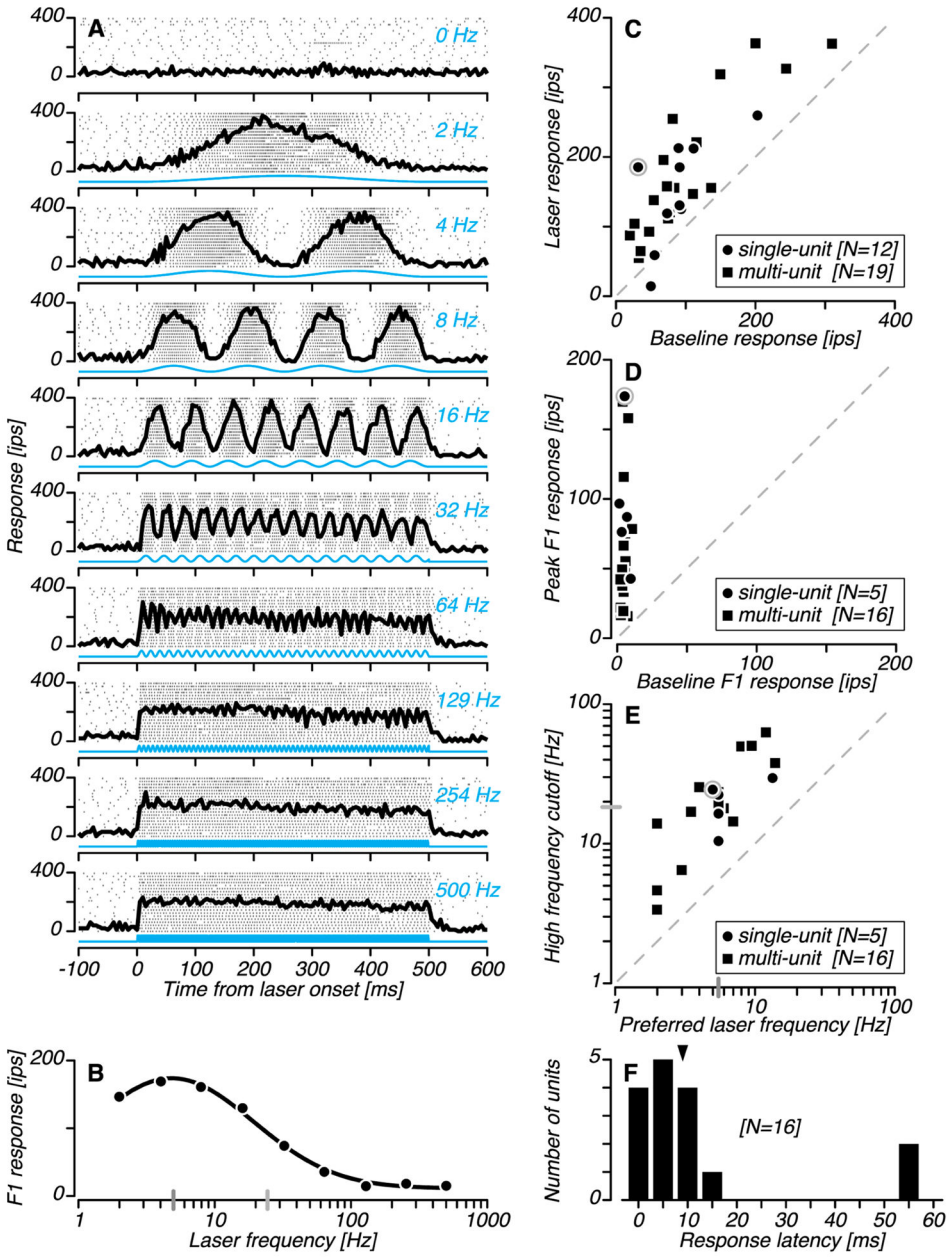

Figure 5.

Optogenetic activation of cerebellar units. **(A)** Rasters (tick marks) and PSTHs (black) for an example single unit tested with nine frequencies of sinusoidal light modulation (blue). **(B)** Response dependence on stimulation frequency for the same example unit. **(C)** Strength of optogenetic activation across all laser modulation frequencies tested. **(D)** Strength of optogenetic activation at the preferred frequency. **(E)** Preferred laser frequencies and high frequency cutoff values. The gray bars passing through the ordinate and abscissa mark the median values across all units. Data for the example unit is encircled in gray in **C–E**. The dashed line is the identity line. **(F)** Latency of optogenetic activation. Distribution of

latencies derived from the responses to 100–500 Hz sinusoidal optical stimulation conditions. The median latency was 9 ms (triangle).

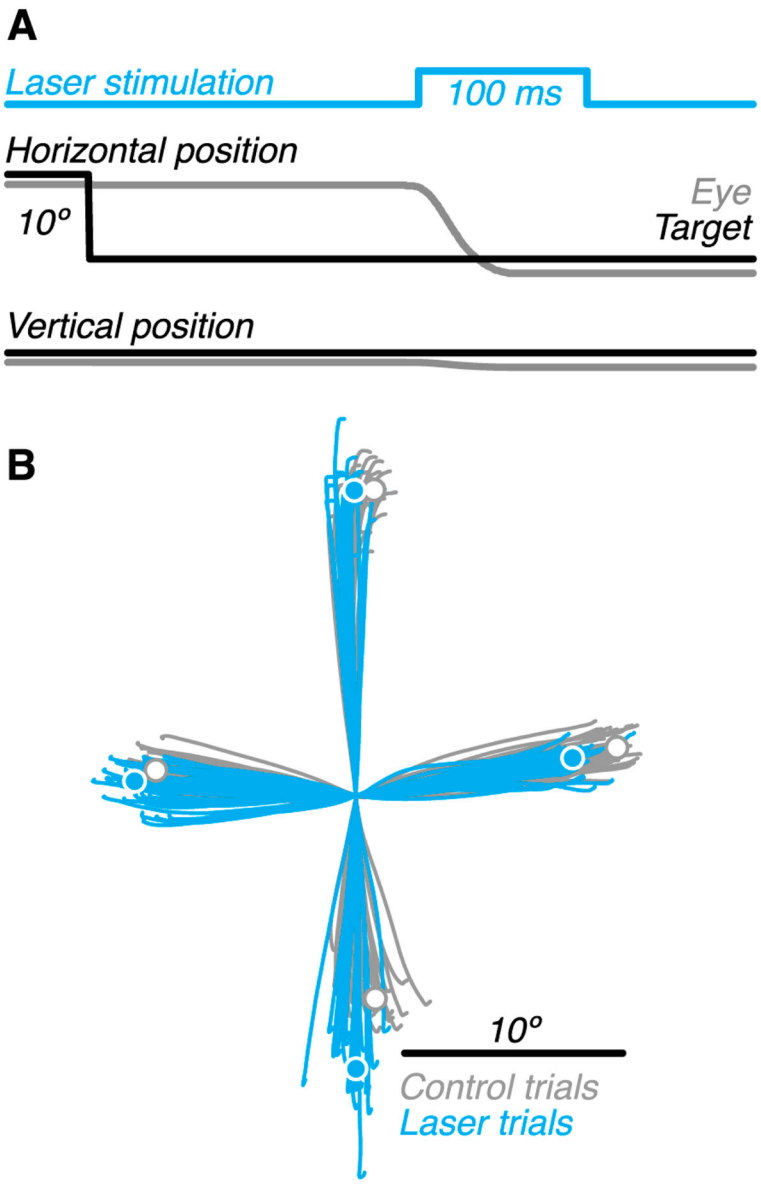

Figure 6.

Effects of optical stimulation on saccade trajectories from one behavioral session. **(A)** Timing of trial events. **(B)** Example saccade trajectories (lines) for control (gray) and laser (blue) trials from a representative stimulation site. Circles represent average saccade endpoints.

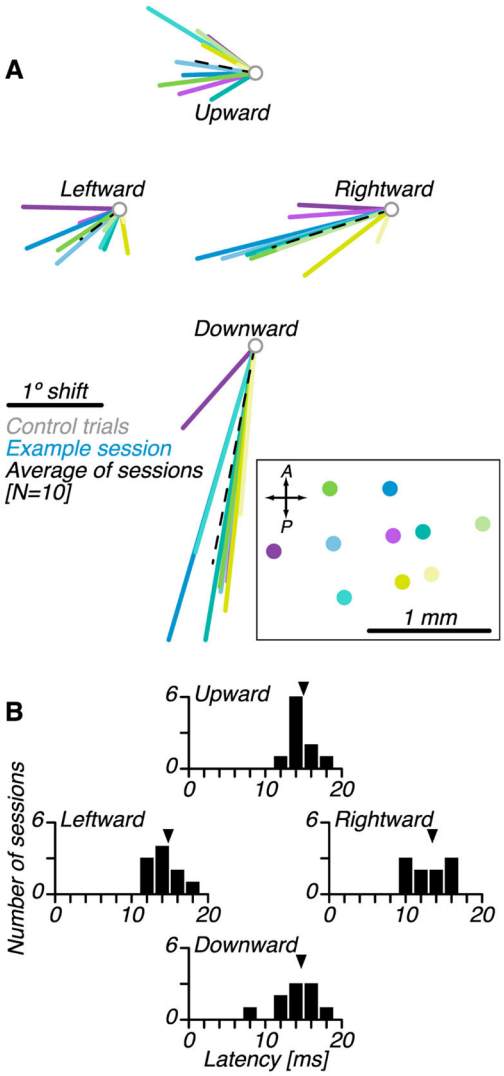

Figure 7.

Effects of optical stimulation on saccade trajectories across all behavioral sessions. **(A)** Average changes in saccade end points for each stimulation site (N=10 stimulation sites, colored lines) and across sites (dashed line). Inset (black box) shows the location of stimulation sites within the recording chamber in the same color code. **(B)** Latency of the first significant change in saccade velocity after stimulation onset (see STAR Methods).

Table 1

Estimates of position and spread of transduced cerebellar regions. Lobules identified based on an anatomical atlas of the rhesus monkey cerebellum (Madigan Carpenter, 1971).

Monkey	Vector	Spread (Anterior–Posterior) Lobule	Spread (Anterior–Posterior) (mean ± S.D.)	Position (Medial–Lateral)	Spread (Medial–Lateral)
1	AAV9–L7	IIIb	2.4 ± 0.1 mm	~6 mm	~5 mm
2	AAV9–L7	II	3.1 ± 0.1 mm	~3 mm	~10 mm
2	AAV1–L7	IIIb, IVa	1.9 ± 0.2 mm	~2 mm	~2 mm
3	AAV1–CMV	Vd, Ve, Vf	5.1 ± 0.5 mm	~8 mm	~5 mm
4	AAV9–L7	VIc, VII, VIIIa	6.7 ± 0.8 mm	~0 mm	~8 mm* *patchy expression